

Wind Data Collection and Analyses at Masdar City for Wind Turbine Assessment

Isam Janajreh*, Ilham Talab

Masdar Institute of Science and Technology, Abu Dhabi, P.O. Box 54224, United Arab Emirates

Abstract

Wind turbine technology has improved dramatically in the last two decades and their deployment and implementation increased by 20-25% annually. Wind is neither chaotically generated nor is based on random phenomenon. Wind is predictable to greater extent. Current predictive models lack the validation against collected historical data. In this work a 50m meteorological tower was installed at Masdar City for continuous collection of annual wind data records. Data is sampled at 10 minutes sampling rate using Campbell 1000 data logger connected to cup vane anemometry at 5 different heights to estimate the boundary layer profile. Collected and estimated wind energy density was below 120Watt/m² suggesting low wind area and undermining the feasibility of wind turbine implementation in the city. Data is analyzed for their first (mean and standard deviation) and second moments (correlation and spectrum) and found to vary considerably in scale and time suggesting simultaneous time and scale analysis. Wavelet analysis is used to study the intermittency of the wind data and quantify their intermittency factor.

Keywords: Wind Energy, Wavelet Analysis, Frequency Spectrum

1. Introduction

Wind turbines continue to provide an increasing share of renewable energy generation; there has been an annual growth of between 20 to 30% in the last decade [1]. The carbon dioxide emitted due to their material fabrication is paid back within nine months of their installation [2]. There are, essentially, two types of wind turbines, classified by the direction in which the rotor rotates with respect to the ground. The older generation wind turbines tend to have a lower power and a vertical axis (i.e. anemometer cup, Savonius and Darrieus rotor) while the higher power, horizontal-axis turbines (i.e., Vestas series v15, v27, v39, and v66, Windmaster series 500, 750, and 1000, and Nordex N500) are the ones commercially deployed worldwide.

Evaluation of the wind resource at a given site is the first step in a wind project development process [3]. There is evidence of greater winds along coastlines, caused by sea breezes, than along flat inland areas. A preferable site is one that is privately owned, has reasonable access, close proximity to power transmission lines, and one that is within a receptive community.

Wind turbine metrics are measured by their “rated power” which can be estimated from values of the measured incoming wind speed. It is typically presented in non-dimensional form by the rated power coefficient K_p [4]. This coefficient expresses the ratio between the wind power generated and the power available from the incoming wind [4]. In wind turbine theory, the wind turbine is modeled by a thin disc in the passage of a constant mass flow stream tube. The power is expressed as:

$$P = \frac{1}{2} \dot{m}(u_1^2 - u_2^2) \quad (1)$$

where \dot{m} is the mass flow rate. This is calculated as follows:

$$\dot{m} = \rho u_{disc} A_{disc} = \rho u_1 A_1 = \rho u_2 A_2 \quad (2)$$

Where ρ is the wind density, and A_{disc} , A_1 and A_2 are the disc area, stream tube inlet, and outlet, respectively. The maximum power that can be harnessed by a wind turbine can be calculated using this disc concept such that:

$$P_{max} = \frac{16}{27} \cdot \frac{1}{2} \rho A u_1^3 \quad (3)$$

* Corresponding author. Tel.: +97126988122

Fax: +97126988121; E-mail: ijanajreh@masdar.ac.ae

© 2010 International Association for Sharing Knowledge and Sustainability

DOI: 10.5383/ijtee.01.01.007

It is directly proportional to the rotor swept area (2nd order to the radius) and to the 3rd order of the wind speed. The ratio of the maximum power to that incoming potential power defines the maximum theoretical rated power. It is given as:

$$K_p = \frac{16}{27} \cdot \frac{1}{2} \rho A u_1^3 / \frac{1}{2} \rho A u_1^3 = 0.593 \quad (4)$$

This factor limits the amount of wind energy that the turbine can convert into useful energy. The typical K_p value is near 0.4 [5]. Aerofoil friction drags, wake losses and a definite number of blades are responsible for a rated power that is smaller than the theoretical maximum. There is a compromise between an increase in the rotational speed and the use of fewer blades. It can be extremely useful to simulate this complex problem using numerical simulation at an early conceptual design stage. The recorded mean wind speed of a given site makes it feasible to estimate the wind power density. This is defined as P_{max} per wind turbine swept area. This measure of power density is commonly represented by a line plot, as illustrated in Fig. 1. It indicates the cut-in and cut-out wind speeds, implemented for operational efficiency and safety reasons, and it also displays the rated speed (15 to 25m/s), which is the value at which the turbine produces its rated power.

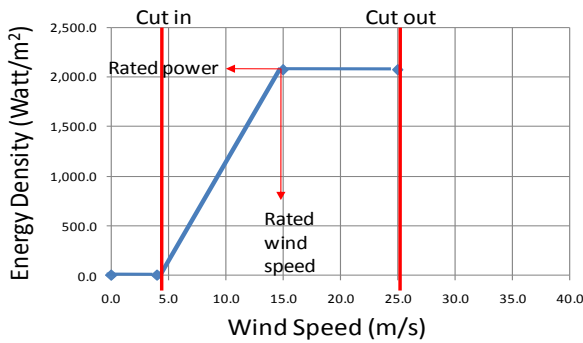


Fig. 1. Illustration of a wind turbine cut-in and cut-out speed.

The production of wind turbines is a competitive market, with companies including companies such as Vestas, Nordex, Siemens, WTC, and GE to name a few. In some developed countries wind energy accounts for over 5% electrical grid penetration, In Germany and Ireland, the grid penetration is 6.3%, and in Spain and Portugal, the grid penetration is 9% [1]. In the eastern gulf region, studies on the operation strategy of wind turbines, wind farms, and the feasibility of hybrid wind power systems continue to promote the implementation of wind turbines in the region. Obtaining the mean wind speed (at two heights, 10m and 50m) presents a meaningful estimate to the wind power density ($p = \frac{1}{2} \rho u^3$). Sites that offer wind speeds of 6m/s can be considered for wind farm implementation and grid integration [6].

Atmospheric boundary layer simulation in a wind tunnel is a complex task. The incoming flow is not parallel and in reality, this layer extends from hundred meters in open terrain to several hundred in urban terrain. It is commonly modeled by the power law described as:

$$u(z) = \begin{cases} U_m (h_{mbl} / H_m)^{\alpha_m} (z / h_{lbl})^{\alpha_l} & z < h_{lbl} \\ U_m (h_{mbl} / H_m)^{\alpha_l} & z \geq h_{lbl} \end{cases} \quad (5)$$

where U_m is the average wind speed at the meteorological tower at elevation H_m , α_m and α_l are exponents characterizing the terrain exposure, and h_{mbl} , h_{lbl} are the estimated boundary layer depths next to the tower. Common values are $H_{met} = 50m$, for 0.16, $\alpha_l = 0.16$, and $h = 100m$. Incoming turbulence and its characteristics (spectrum, intensity, and intermittency) add uncertainty to the wind tunnel data.

Wind analysis is an essential step for a given site wind assessment and wind turbine implementations while numerical analyses are extremely useful in investigating new innovations and in conducting parametric sensitivity studies. This may include downwind turbines and tower rotor interaction, rotor winglets integration, and rotor pitch angle optimization to name a few. Nevertheless, wind turbine numerical simulations are computationally intensive and there is trade between accuracy and time reduction. Utilization of High Performance Computations (HPC) is becoming normal practice that allows construction of high fidelity full scale models and at the most affordable special and temporal resolutions.

2. Objective and Motivation

The objective of this work is to assess the wind turbine implementation at Masdar city site located in UAE at 24.4202° N latitude and 54.6132° E longitude. To achieve this objective, a 50m tubular meteorological tower was installed at the Masdar city site to collect continuous records of wind over a year since August 1st 2008. The mast is equipped with 5 calibrated Hersteller Thies Cilma cup anemometers [7], two wind vane, one Campbell CR100 data logger, and three sensors to each of Temperature, Barometric pressure and humidity measurements. It records five velocities (at 10m, 30m, 40m, 49m, and 50m), two directions (at 30m, and 50m) as well as pressure, relative humidity, and temperature at 50m. Wind records are sampled at 10Hz and averaged over 10 minutes. The values are obtained continuously through the year at every 10 minutes interval from August 2008 through Feb 2009. Wavelet analysis which is more suitable to study intermittent and time varying non-stationary data will be used to conduct data analysis. Correlation between the resulted velocities at the five heights will be investigated and their projected temporal energy density is presented.

3. Wind Data in the Eastern Gulf Region

The Arabian Peninsula eastern coastlines experience relatively a low level of wind that varies from one season to another. In Dhahran (26°32' N, 50°13' E, eastern coastal plain of Saudi Arabia), the yearly average wind speed is nearly 4.3 m/s and its energy density is 89 watt/m² in the period of 1986-1998 [6] as depicted in Fig. 2.a. The monthly average wind speed also varies between 4m/s and 6.5m/s with an average speed of 5.1m/s as depicted in Fig. 2.b [6]. The estimated energy density for these wind speed records is averaged near 90watt/m² and it varies considerably during the year. The data suggest that the eastern side of peninsula is located at the borderline of the cut-in wind turbine speed ($\approx 4.5m/s$) of several widely deployed wind turbine brands. This emphasizes that a lower turning moment and thereby a lower cut-in speed wind turbine is the ideal choice for the eastern gulf region. The Masdar city in Abu Dhabi located at 24.4202° N latitude and 54.6132° E longitude exhibit a low level of daily average wind speed as

shown in Fig. 2.c. The collected high resolution time-scale varying data at the Masdar city is suitable for scale/time wavelet analysis avoiding the classical Fourier spectrum/components as illustrated below.

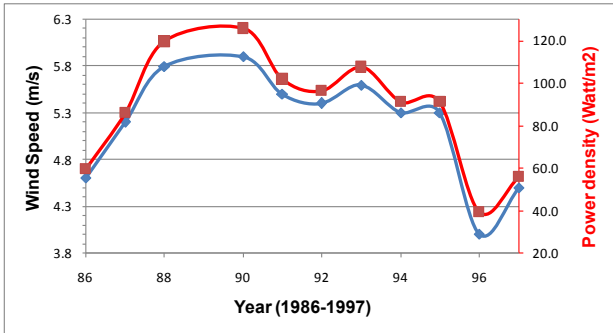


Fig. 2a. Yearly average wind speed and energy density in Dhahran^[6]

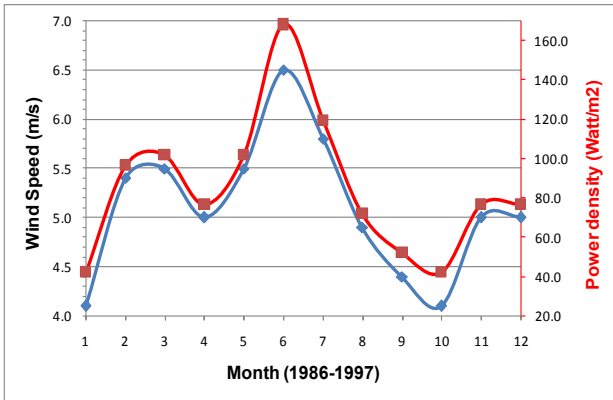


Fig. 2b. Monthly avg. wind speed at Dhahran (1986-1997 period)^[6]

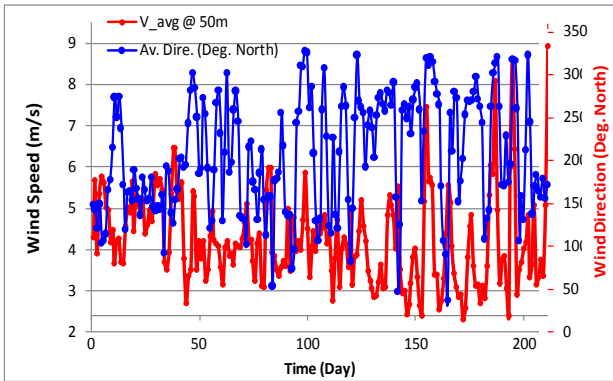


Fig. 2c. Monthly avg. wind speed and direction at Masdar city (August through February period)

3.1. Wavelet Analysis of Non-stationary Data

When a signal exhibits time varying spectral characteristics, it is said to be non-stationary. For such signals, a conventional spectral analysis based on Fourier transforms is of limited value. The non-stationary signal should be described in a time-frequency or time-scale plane. Such representation can be obtained by using a wavelet transform. Given a time series $f(t)$, its continuous wavelet transform is defined as:

$$\omega(a, \tau) = a^{-\frac{1}{2}} \int_{-\infty}^{+\infty} f(t) \psi^* \left(\frac{t-\tau}{a} \right) dt \quad (6)$$

Where $\omega(a, \tau)$ are the wavelet coefficients, $\frac{1}{\sqrt{a}} \psi \left(\frac{t-\tau}{a} \right)$ are basis functions called wavelets and the * indicates complex conjugate. The above transform is represented in terms of the scale a and the time τ parameters. The wavelets, ψ , are scaled and translated (by varying a and τ) versions of the basic wavelet type, referred to as a mother wavelet. The wavelet is admissible; this property guarantees that if a function of time is transformed into the time-scale domain with that wavelet, then the inverse transform exists. The wavelet transform is the projection of $f(t)$ onto all scaled and translated versions of the single mother wavelet, $\psi(t)$. Thus, $\omega(a, \tau)$ represents the relative contribution of scales a to the signal at time τ . For discrete data, practically speaking, both a and τ need to be discrete as well. A general form of the discrete wavelet transform is obtained by selecting $a = a_o^m$ and $\tau = n \tau_o a_o^m$, where a_o and τ_o are constants that represent the base scale. The time resolutions ($a_o > 0$ and $\tau_o > 0$) and the indices m and n are integers. Appropriate discretization of a and τ allows one to choose a basic wavelet and obtain a set of orthonormal bases which will be used in this work. Daubeshies [8], and Meyers [9] invented an algorithm that provides such a base function. For example if a_o is chosen to be 2 and $\tau_o = 1$, the analysis done octave by octave, one could obtain an orthonormal basis for a certain $\psi(t)$. Consequently the function $f(t)$ can be approximated by a linear combination of the wavelets, i.e., one can write:

$$f(t) = \sum_{m=0}^{\infty} \sum_{n=0}^{2^m-1} \omega_m[n] \psi_{m,n}(t) \quad (7)$$

where the wavelet coefficients $\omega_m[n]$ represent the contribution of scale 2^m over time $n2^m$. By letting

$$\psi_{m,n}(t) = 2^{-m/2} \psi(2^{-m}t - n) \quad (8)$$

one can rewrite (7) as:

$$f(t) = \omega_o + \sum_{m=0}^{\frac{\log N}{\log 2} - 1} \sum_{n=0}^{2^m-1} \omega_{2^m+n} 2^{-\frac{m}{2}} \psi(2^{-m}t - n) \quad (9)$$

where ω_o is the signal mean value. Based on the last two equations one can compute the discrete wavelet coefficients as:

$$\omega^m[n] = \sum_{-\infty}^{+\infty} 2^{-m/2} \psi(2^{-m}t - n) f(t) \quad (10)$$

Squaring both sides of (7) and integrating over the time domain results in the means-square value of $f(t)$. By reducing this value by orthonormal wavelets, one obtains:

$$\int_{-\infty}^{+\infty} f(t)^2 dt = \omega_o^2 + \sum_{m=0}^{\log N} \sum_{n=0}^{2^m-1} \omega_{2^m+n}^2 2^{-\frac{m}{2}} \psi\left(\frac{1}{2^m}\right) \quad (11)$$

Expanding leads to:

$$\int_{-\infty}^{+\infty} f(t)^2 dt = \omega_o^2 + \omega_1^2 + \frac{1}{2}(\omega_2^2 + \omega_3^2) + \frac{1}{4}(\omega_4^2 + \dots + \omega_7^2) + \frac{1}{8}(\omega_8^2 + \dots + \omega_{15}^2) + \frac{1}{16}(\omega_{16}^2 + \dots + \omega_{31}^2) + \dots \quad (12)$$

The equation shows the contributions to the mean-square value of a signal from all scales. The Daubeshies wavelets are used to examine time-varying characteristics of the atmospheric wind. Duabeshies wavelets are specified by a particular set of wavelet filter coefficients, 2, 4, 6, 8 or 20, ranging from highly localized to highly smooth. Fig. 3 shows wavelet functions along with their Fourier transform. One should note that as the number of filter coefficient increases, the wavelet becomes smoother and ultimately becomes closer to a harmonic window as it becomes less local.

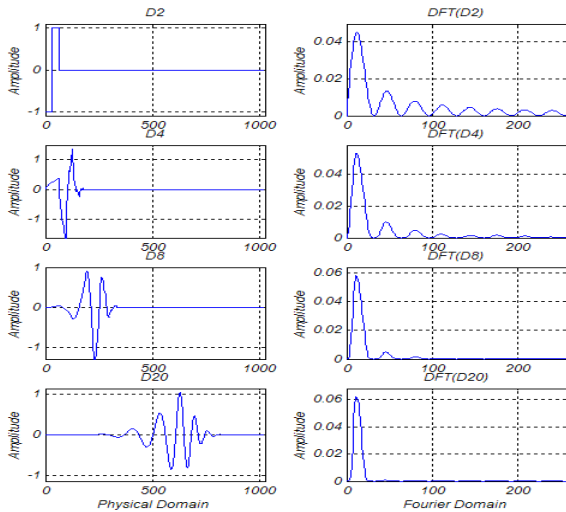


Fig. 3. Daubeshies D2, D4, D8, and D20 wavelets and their Fourier-Domain Transforms.

3.2. Scale Energy Representation

To illustrate how wavelet analysis works, a discretely sampled function shown in Fig. 4 is investigated. It is given by:

$$f(t) = \begin{cases} 1.0 + \sin(2\pi \frac{t}{127}) & : 0 \leq t \leq 127 \\ 0.5 + \text{uniform}(\text{rand}) & : 128 \leq t \leq 256 \\ \sin(2\pi \frac{20(t-257)}{255}) & : 257 \leq t \leq 512 \\ 1.0 + \sin(2\pi \frac{20(t-257)}{255}) \sin(2\pi \frac{12(t-513)}{255}) & : 513 \leq t \leq 768 \\ 1.0 + \sin(0.2(2\pi \frac{20(t-768)}{231}))^3 & : 767 \leq t \leq 1000 \\ 1.0 & : 1001 \leq t \leq 1024 \end{cases} \quad (13)$$

The function consists of a large- and small-scale oscillations, random fluctuations, amplitude and frequency modulations and constant at a signal mean value of one unit.

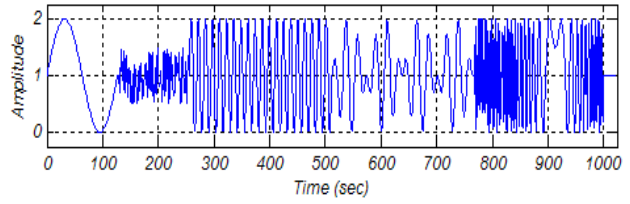


Fig. 4. Sampled function of different frequencies and times.

The physical domain is mapped into a record that spans over $2^{10}=1024$ units. Fig. 5 shows the D4 decomposition over $\frac{\log 1024}{\log 2} + 1 = 11$ scales.

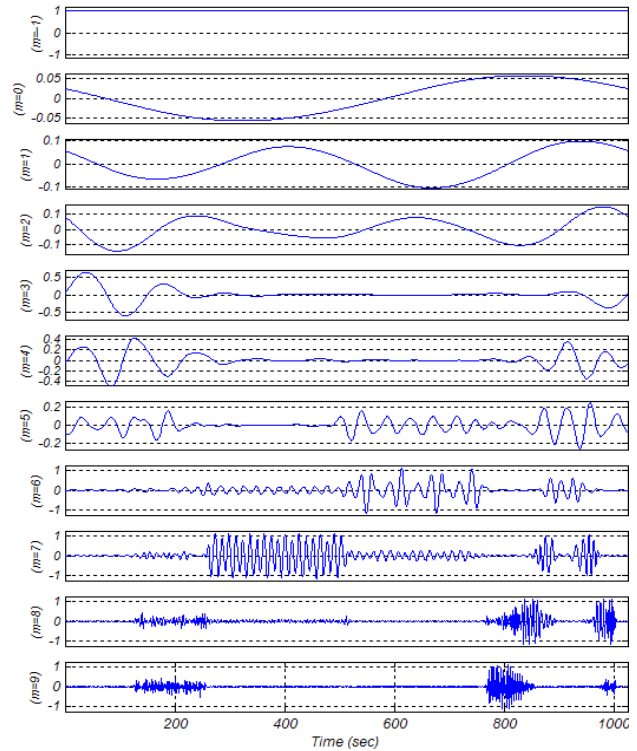


Fig. 5. Decomposed 11 levels of the time series signal.

Where the additional scale represents the signal mean and is denoted by $m=-1$ level. The second, denoted by $m=0$, represents the largest signal scale and is obtained by projecting one wavelet over the whole signal. The third scale denoted by $m=1$, is obtained by projecting two wavelets onto the signal. This projection is continued until the eleventh scale, denoted by $m=9$, is obtained by applying 512 wavelets onto the signal. As expected, level -1 has a value of 1 which is exactly the mean signal value. At $m=3$ the wavelet catches the largest signal scale which is defined over $0 \leq t \leq 128$; the random segment which contains several frequency components, as expected, is captured in several scales $m=3$ through $m=9$. The high frequency segment $257 \leq t \leq 512$ is captured by scale $m=7$ and the amplitude modulation of the signal is captured at $m=6$ and $m=7$ and with some residual to the signal scales that appears in one higher or lower scale due to the wavelet-signal mismatch. Higher sampling rate typically fixes this mismatch. Frequency modulation at $767 \leq t \leq 1000$ is best captured by several successive scales $m=6$ through $m=9$ at different times that slides at a rate proportional to the modulations. The constant however is seen as large oscillations and captured by the largest scale $m=1$ through $m=4$. Fig. 6 shows the

reconstructed signal obtained by adding the successively transformed scales where it is obvious that such a signal can be satisfactorily constructed from the wavelet coefficients.

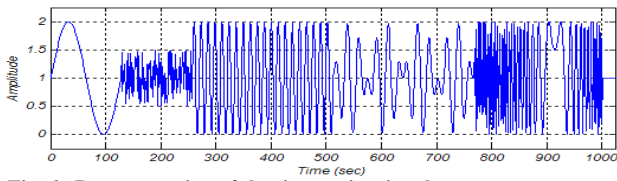


Fig. 6. Reconstruction of the time series signal.

The energy of each scale is presented by the square of the wavelet coefficient. The time variation of this energy maps their magnitudes over all the eleven scales at all times and when it shows a significant magnitude it corresponds to the presence of a certain scale in the signal. Adding the energy over times will give the total energy content of a certain scale as shown in Fig. 7.

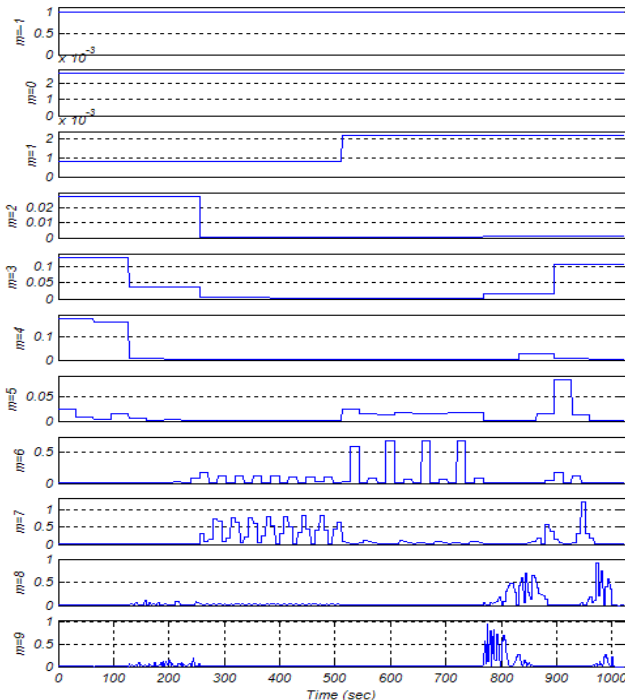


Fig. 7. Energy representation of the time series signal.

3.3. Intermittency Representation

Intermittency is, in general, defined as the occurrence of short-time irregular variations in a long regular signal. It is the time fraction of “turbulence” versus “non-turbulence” or can be identified by the measuring device when a variation in a high energy state is detected. Consequently, intermittency can be measured as a time factor or percentage. To illustrate this, Fig. 8 (a) represents a sinusoidal time series, and in Fig. 8 (b) a short-time variation to the signals was added.

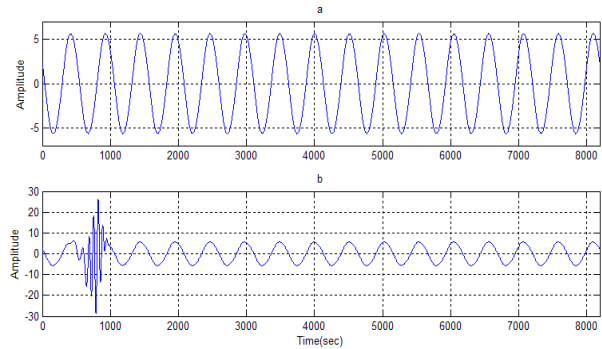


Fig. 8. Intermittent time series signal.

We computed the wavelet coefficients of both signals and calculated the average energy of all scales. To quantify the intermittency, the following approach is taken: when the measuring devices detect the scale’s energy at a higher state than a certain threshold, the scale is considered to be intermittent. This threshold has been defined as twice the average energy of that scale. This measure, in addition to the scale energy contribution, produces a complete picture of the intermittency. The significance of these results is that they reveal the level of intermittency of energetic scales. A highly intermittent scale could be insignificant if its contribution to the total energy is negligible. Fig. 9 shows the intermittency factor and energy percentage contribution of each scale for the signals given in Fig. 8. As expected, the intermittency factor is zero for the sinusoidal signal and its total energy is captured in the 4th scale. The addition of a smaller scale to the sinusoidal signal over 2.34% of the time, has an associated intermittency of 2% and is recorded at the 7th scale as shown in Fig. 9. The total energy of the signal is divided between the periodic scale (73% contribution) and the intermittent scale (27% contribution).

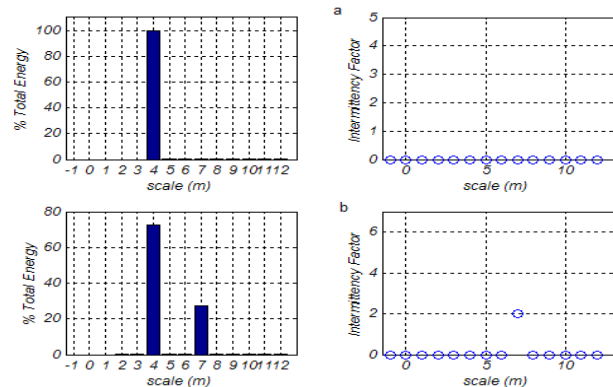


Fig. 9. Intermittency factor and energy percentage contributions corresponding to the two signals of Fig. 8.

3.4. Initial Investigation of Masdar city Wind Data

Time evolution of wind data at Masdar city is presented in Fig. 10. The mean wind data for the 7 months period at the four heights are summarized in Table 1 below along with the wind direction at heights of 50 and 30 m.

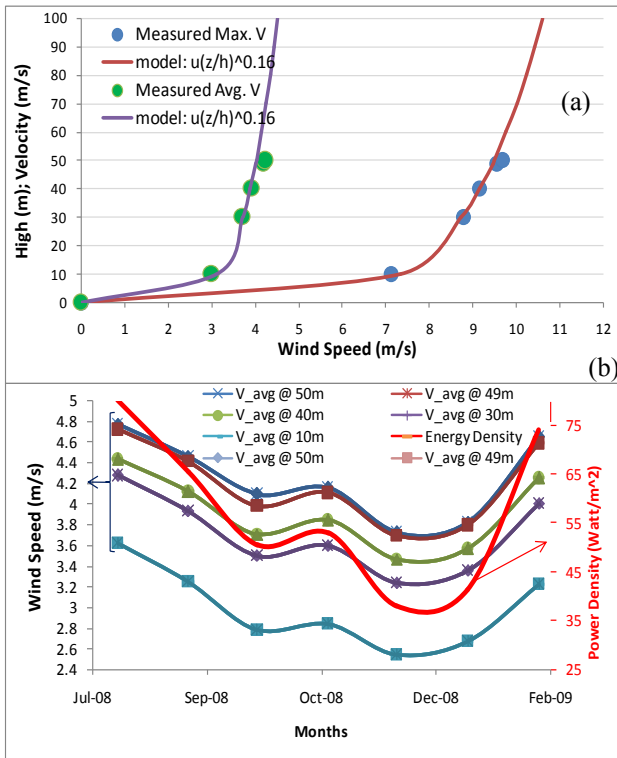


Fig. 10. Measured velocity and power law data (a) and monthly average and energy density data (b).

Table 1. Summary of the Average Wind Speed, Direction, and Corresponding Wind Power Density at Masdar City

Height	50	49	40	30	10
Avg. Wind Speed (m/s)	4.25	4.20	3.92	3.70	3.00
Avg. Wind Direction. (Deg. North)	205.00	n/a	n/a	205.00	n/a
Power Density (Watt/m ²)	56.42	54.45	44.27	37.23	19.85

The average wind speed is near the cut-in wind speed of the commonly used Vestas and GE series as summarized in Table 2. The maximum daily wind speed over a few days reaches 8.5m/s. The wind at Masdar city travels in an east western direction. A wind direction distribution of the wind can be seen in Fig. 11. Note that the relative distance of each point in Fig. 11 from the centre is equivalent to the number the associated wind direction occurred. An appropriate power law model for the data at a given instant of time, can be presented assuming a typical open terrain exponential ($\alpha=0.16$) and boundary layer thickness (100m). The velocity profiles would indicate a mean wind speed of 4.5m/s and a maximum wind speed of 10m/s. The monthly average speed at the four measurement heights are well correlated as depicted in Fig. 10b. It should be emphasized that the power density corresponding to the 50m height is less than 60 Watt/m², which is lower than the values (120 Watt/m²) observed in Dahrhan city [6]. From this figure and based on the power law, it can be estimated that it will be more desirable to install a wind turbine at a height of 80m height if it is to be running continuously.

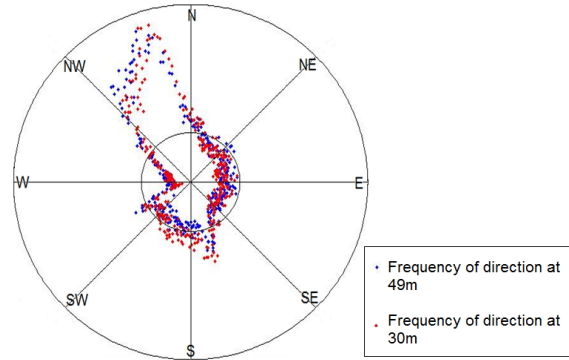


Fig. 11. Wind direction distribution of Masdar city wind data from August to February.

Table 2. Metrics of some Vestas and GE wind turbines

Wind Turbine Model	Rated power (kW)	Rated Speed (m/s)	Cut-in/Cut-out Speed (m/s)	Rotor Dia. (m)	Hub height(m)
Vestas 52-850	850	16	4.0/25.0	52	44, 49, 55, 65, 74
Vestas 82-1.65	1650	13	3.5/20.0	82	70, 78, 80
GE 1.5 sle	1500	14	3.5/25.0	77	65, 80
GE 1.5 xle	1500	11.5	3.5/20.0	82.5	80

In order to choose appropriate analysis method for the wind data, first and second order moments are evaluated. This includes evaluation of the mean, standard deviation and correlation coefficients, as well as the spectra for different lengths of the wind data. The first moment analyzes the data in the time domain and is an example of linear regression analysis whereas the second moment uses the frequency domain. The wind speed data from a height of 50m is analyzed. It is observed that the mean value and standard deviation do not remain constant as the size of the data set under evaluation is increased as summarized in Table 3. The correlation coefficient for seven days of data is calculated through comparison of the first seven days and second seven days within the data set. This is the same procedure applied for the other correlation coefficient calculations. A correlation coefficient of 1 would indicate data of a stationary and predictable nature.

Table 3. Time-domain analysis for different lengths of wind data from Masdar City.

Days worth of data	Mean (m/s)	Standard Deviation	Correlation Coefficient
7	5.093	1.868	0.284
14	4.644	2.127	0.422
28	4.729	2.126	0.331
56	4.687	2.159	0.270
112	4.400	2.036	0.141
224	4.208	2.041	-

Note: For 7 days worth of data, the analysis is applied to the first seven days within the data set. This is the same procedure applied for the analysis of the other data set lengths

The widely varying results for the mean, large standard deviation values and low correlation coefficient values would indicate that the data is non-stationary. It is, however, insufficient to verify whether or not a data set is non-stationary by simply analyzing the data in the time domain. It is also necessary to evaluate the data set in the frequency domain. A

number of frequency spectrums, utilizing different data set lengths can be seen in Figs. 12a and 12b.

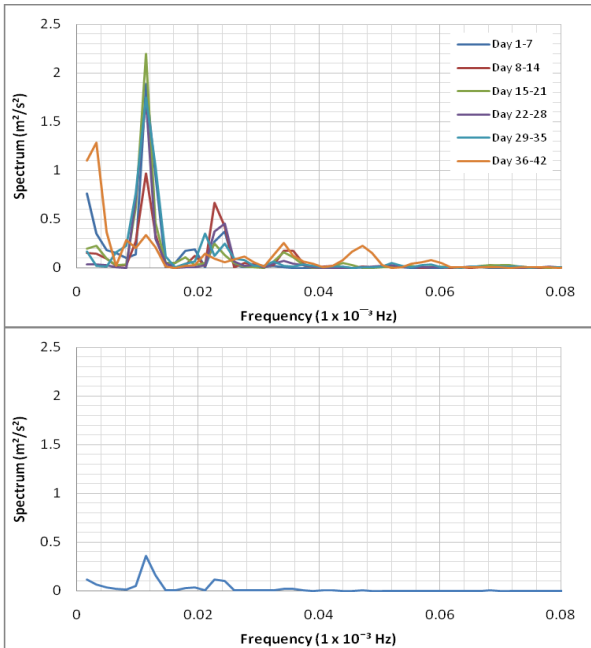


Fig. 12a. Frequency Spectrum (left) & Average frequency of 30 spectrums (right) for wind speed data from Masdar City. 7 days data length.

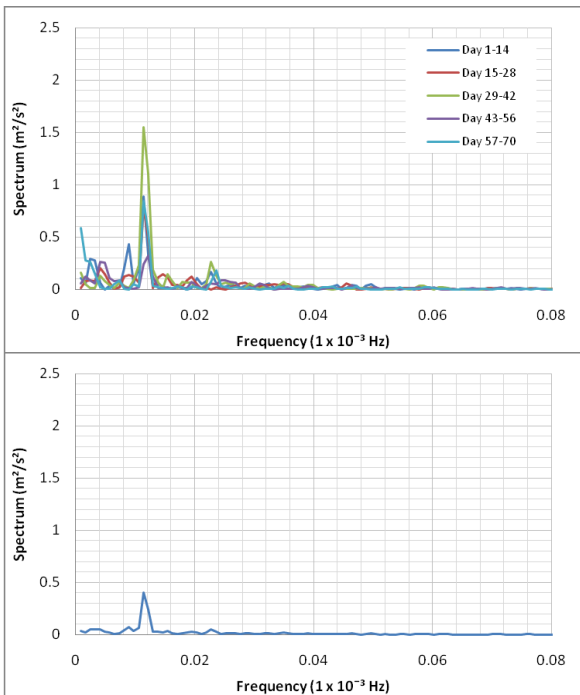


Fig. 12b. Frequency spectrum (left) & Average frequency of 8 spectrums (right) for wind speed data from Masdar City. 14 days data length.

It can be observed that the peaks vary greatly from one frequency spectrum to another. These peaks are smoothed and reduced in magnitude upon averaging, as can be seen in Fig. 12a (right). Use of this spectral analysis alone for the prediction of the wind speed would therefore generate highly inaccurate results. There does however appear to be peaks at approximately the same frequencies, at 0.21×10^{-4} Hz and 0.23

$\times 10^{-4}$ Hz. This suggests that even though the data may be non-stationary it is not entirely unpredictable. A wavelet analysis can therefore be tested.

Wavelet analyses are used here following the previous procedures to observe the trend of the temporal data (10minutes/sample) more willingly than studying the turbulence wind-eddies or wind-gusts that essentially last a few seconds and require higher sampling rate. Wind turbulence is beyond the scope of this work, it was exclusively treated with wavelet in previous work to the author [10]. The wavelet representations of the wind speed for the two months August and January is captured in Fig. 13 including the percentage of total energy contained in each scale, the intermittency factor and the percentage of energy contained during intermittent events. By examining the energy content of different scales for each month (August through February), it is noticed that the percentage of total energy contained in each scale varies with time. This variation implies these monthly records for the wind data are not stationary as suggested earlier. Yet, one should note that in general most of the energy is contained in the 5th to 7th scale with, somewhere, 15% to 30% of total energy of the signal and are not evenly distributed. The August month energy is contributed by the 5th though the 7th scale, while January adds the contribution of the 2nd and 3rd scales.

The intermittency factor gives the percentage of time the wavelet coefficient of a particular scale is larger than twice its average value. The results show that scales 2 through 7 have consistently an intermittency factor between 12% and 25%. Besides measuring the intermittency factor, the percentage of the total energy of each scale contained during the intermittent events. The results show that about 60 to 70 percent of the energy of each scale appears in less than about 15% to 25% of the time. This is of great importance for characterizing the wind at this relatively coarse sampling rate. That suggests most of the wind energy of different scales appear in a short period of time.

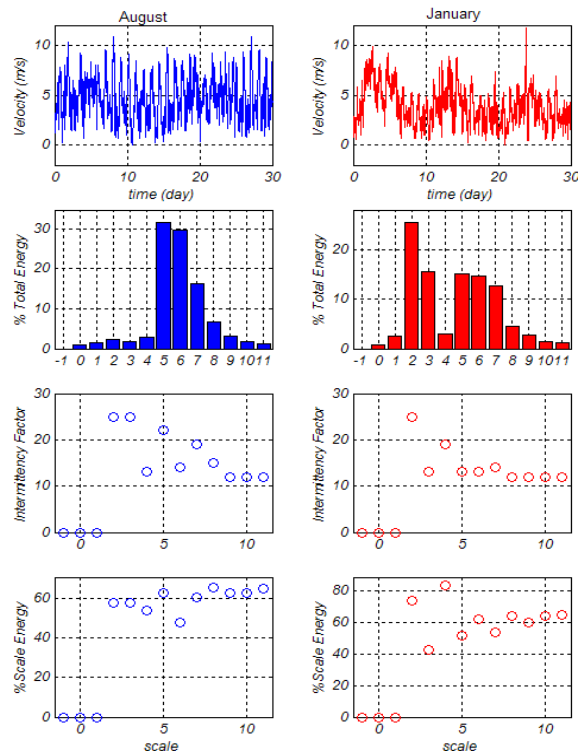


Fig. 13a. Total energy, Intermittency factors, and % Intermittency energy in scales.

The energy contents in the different scales in the wind direction signal exhibit more intense variation than that of the speed. The higher scales are energetic as well. The most of the energy is contained in the same scales 5th through 7th however it is slightly more distributed. The intermittency factor for the wind direction shows between 12% to 25% for the 4th and above scales. These scales are contributing somewhere between 40 to 80% of their energy within this time interval. This substantiates the non stationary characteristics of wind data and at Masdar city in particular located in the gulf region. Furthermore, the time-scale results can be used to generate a representative wind data records from limited observations (via inverse wavelet transform) based on which wind turbine energy density can be estimated.

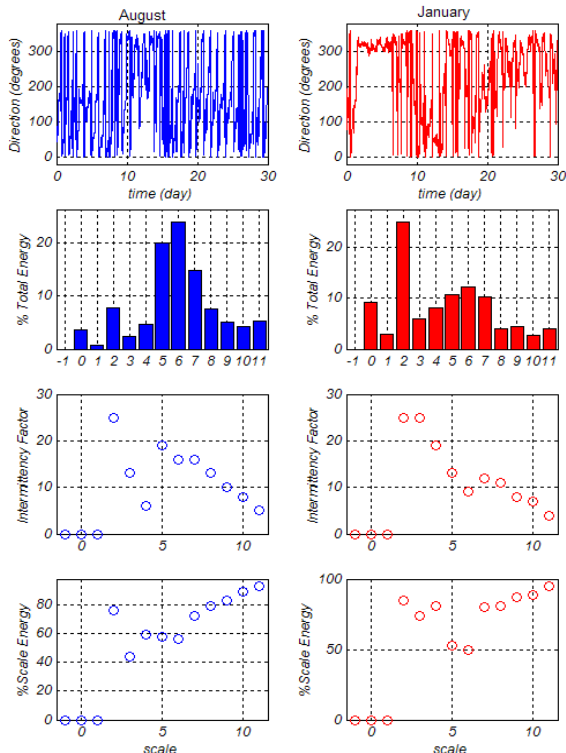


Fig. 13b. Total energy, Intermittency factors, and % Intermittency energy in scales.

4. Conclusion

Wind turbine implementation is reviewed in this work. Site investigation and estimation of the energy density and flow characteristics utilizing wavelet analyses was carried out. The investigation concluded the non-stationary and highly intermittency of wind speed and its direction and introduced a method to quantify it. It also shows the low density level of the continuous 7 months collected wind records at the Masdar city which fall in class 1 poor to fair wind speed. The results show that the power density corresponding to the 50m height is less

than 60 Watt/m² and is lower than the values (120 Watt/m²) observed in Dahrhan city. Therefore, only wind turbine with a low turning moment and characterized with a low cut-in wind speed can be “wisely” implemented in the Masdar city in UAE. Therefore, it would only be wise to implement wind turbines with low turning moments and low cut-in speeds at the Masdar city in UAE. The possibility of analyzing the wind at a height beyond that of the restricted height, (70m due to airport proximity) will need to be explored.

Acknowledgments

The authors would like to acknowledge Jill Macpherson (University of Edinburgh), an intern at Masdar Institute, for her contribution to this paper.

References

- [1] R. Thresher, M. Robinson and P. Veers. The Status and Future of Wind Energy Technology. *J. of Physics of Sustainable Energy*, 978-0-7354-0572-1, 2008.
- [2] Vestas Report. Life Cycle Assessment (LCA). Wind turbine and the environment. 2004. www.vestas.com.
- [3] UAS-GAO on RENEWABLE ENERGY. Wind Power’s Contribution to Electric Power Generation and Impact on Farms and Rural Communities. GA0-04-754, Sep 2004.
- [4] Betz, A. Introduction to the Theory of Flow Machines. (D. G. Randall, Trans.) Oxford. Pergamon Press. 1966.
- [5] M. M. El-Wakil. Power Plant Technology: College Custom Series. Mc Graw-Hill Companies, Inc., 1984 ISBN 0-07-287102-4.
- [6] M.A. Elhadidy, S.M. Shaahid. Wind resource assessment of eastern coastal region of Saudi Arabia. *Desalination*. 209, 199-208. 2007. <http://dx.doi.org/10.1016/j.desal.2007.04.029>
- [7] Deutsche WindGuard Wind Tunnel Services GmbH, MEASSNET 09 1997 – Cup Anemometer Calibration Procedures.
- [8] I. Daubechies, 10 Lectures on Wavelets, S.I.A.M., 1992.
- [9] Y. Meyer, Wavelets: Algorithms and Applications, S.I.A.M., 1993.
- [10] Isam M. Janajreh. Wavelet Analysis of Extreme Wind Load on Low-Rise Structures. Ph. D. Thesis, Jan. 1998. Virginia Tech.